Research Square

Preprints are preliminary reports that have not undergone peer review.
They should not be considered conclusive, used to inform clinical practice,
or referenced by the media as validated information.

Development of nanocrystalline Sr12Al14O33 and Ca12Al14O33 soot oxidation catalysts

Anton P. Koskin

koskin@catalysis.ru

Boreskov Institute of Catalysis

Ekaterina I. Shuvarakova

Boreskov Institute of Catalysis

Alexander F. Bedilo

Boreskov Institute of Catalysis

Research Article

Keywords: Soot oxidation, Mayenite, Oxygen radicals, C12A7, S12A7

Posted Date: September 3rd, 2026

DOI: https://doi.org/10.21203/rs.3.rs-10696378/v1

License: This work is licensed under a Creative Commons Attribution 4.0 International License.
Read Full License

Additional Declarations: No competing interests reported.

Development of nanocrystalline $Sr_{12}Al_{14}O_{33}$ and $Ca_{12}Al_{14}O_{33}$ soot oxidation catalysts

Anton P. Koskin*, Ekaterina I. Shuvarakova, Alexander F. Bedilo

Boreskov Institute of Catalysis, Novosibirsk, Russia

*Corresponding author: *koskin@catalysis.ru*

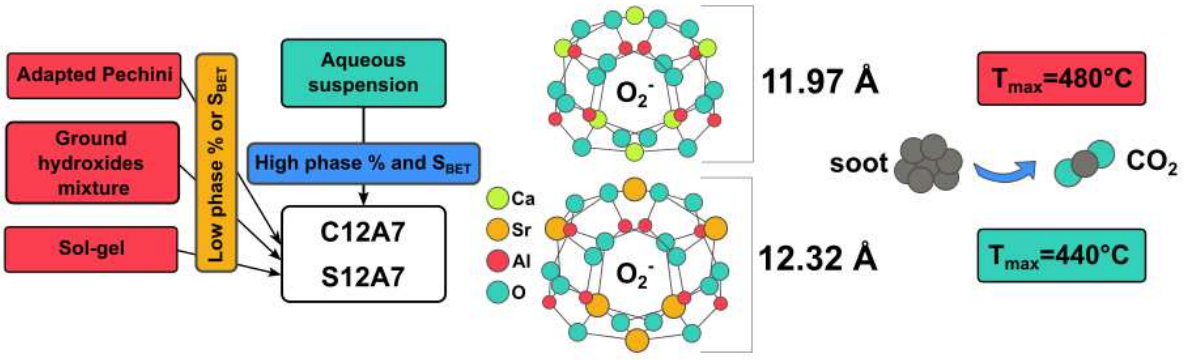
Abstract

Methods for synthesis of nanocrystalline mayenite ($Ca_{12}Al_{14}O_{33}$) and its Sr analog ($Sr_{12}Al_{14}O_{33}$) at moderate temperatures for use as oxidation catalysts were analyzed. Grinding of hydroxides led to the desired phases after calcination, but these samples had very low surface areas. The most promising results were obtained using the reactions of CaO or SrO with water in the presence of a commercial AlOOH sample. Mayenite and its Sr analog were the predominating crystalline phases in the samples prepared by this method after calcination at the temperature as low as 600 °C. It was shown by EPR that these samples had active radical species on the surface after activation in air. Their oxidative activity was tested in the temperature-programmed soot oxidation. They proved to be much more active than the alumina sample used as a reference. The $Sr_{12}Al_{14}O_{33}$ sample demonstrated the highest activity with the CO release peak at 440 °C, apparently, due to its wider crystalline cell and, consequently, enhanced mobility of extra-framework oxygen radical anions.

Keywords

Soot oxidation; Mayenite; Oxygen radicals; C12A7; S12A7

Graphical abstract



1. Introduction

Reducing particulate matter emission from diesel engines is one of important objectives for environmental protection. Such emission is primarily composed of soot particles and can cause serious environmental and health problems. Typically, diesel soot particles are removed from the exhaust gases using methods that combine the use of particulate filters and oxidation catalysts, which are most commonly based on supported noble metal nanoparticles [1, 2]. The efficiency of decomposing soot particles is directly related to the oxidation activity of the catalysts [3].

Catalytic soot oxidation is a complex process that occurs at the interface of the three phases (catalyst, soot and the gas mixture). The catalytic activity in soot oxidation is strongly influenced by two main features: the quality of contact between the soot particles and the catalyst, as well as the transfer of reactive oxygen species (O_2^- and O^-) from the surface of the catalyst to the soot particle with its subsequent oxidation into less harmful molecules such as CO_2 [1, 4].

It is generally desirable to develop cost-effective catalysts based on cheaper components avoiding the use of noble metals where possible. The most popular materials studied as soot oxidation catalysts that can be used without noble metals are based on ceria and perovskites [1, 2, 4-6]. Catalysts based on calcium aluminates with the mayenite structure prepared by assisted solution combustion synthesis were also reported to demonstrate catalytic activity in soot oxidation processes [7, 8].

Mayenite is a calcium aluminate with the composition $12CaO \cdot 7Al_2O_3$ ($Ca_{12}Al_{14}O_{33}$ or C12A7 in the cement notation) that is known for a long time as a component of cements [9, 10]. Its strontium analog (S12A7) was later produced synthetically [11]. These materials feature very unusual crystalline structure (I-43d, Z = 2, a(Ca) = 11.97 Å, a(Sr) = 12.32 Å) [12, 13]. Their unit cells are composed of three-dimensional positively charged frameworks $[Ca_{24}Al_{28}O_{64}]^{4+}$ and $[Sr_{24}Al_{28}O_{64}]^{4+}$. Due to their structural similarity, both materials will be hereafter referred to as mayenite, although this name is commonly used only for C12A7.

In mayenite calcined at moderate temperatures, the charge of the framework is compensated by OH^- anions, which are weakly bound by electrostatic interactions. Their decomposition at elevated temperatures leads to the formation of the oxygen form where irregularly placed oxygen anions O^{2-} act as counter ions. They can be relatively easily replaced by many other anions, including more active forms of oxygen (O^-, O_2^-, O_2^{2-}) [14-18]. The ability of stabilizing oxygen radical anions, electrons or hydride ions inside the framework makes mayenite a promising material for use in various catalytic processes [8, 10, 19-26]. In particular,

mayenite is interesting for oxidation catalysis that can be used both as a catalyst and as a support for active metals due to the presence of extra-framework oxygen radical anions.

The traditional synthesis of mayenite was carried out by the ceramic route using a solid-phase reaction between $CaCO_3$ and γ-Al_2O_3 at temperatures above 1300 °C [27]. Materials prepared by this method are characterized by large crystallite sizes and very low specific surface areas (~1 m^2/g) that are hardly acceptable for catalytic applications. Therefore, many studies were aimed at finding synthesis methods for producing porous nanocrystalline C12A7 under milder conditions. In particular, sol-gel methods [28-30], various modifications of the Pechini method [31-33], production from hydroxide precursors [34-37] and SRS methods [7] were studied. In our group, a method based on the CaO interaction with an aqueous suspension of pseudoboehmite (AlOOH) without the use of additional templates and auxiliary stages of mechanical activation and hydrothermal treatment was recently suggested for the synthesis of finely dispersed C12A7 [29, 38, 39]. Subsequent calcination of the sample at 500-600 °C made it possible to obtain the C12A7 crystal structure with a relatively high mayenite phase content (> 70% according to the XRD data [39]) while maintaining high specific surface area.

The strontium analog of mayenite ($Sr_{12}Al_{14}O_{33}$) has been studied less than C12A7. However, it was suggested that the use of Sr12A7 in oxidative catalysis might be preferable [12]. The O_2^--S12A7 structures presumably can have higher oxidizing capacity due to the larger unit cell cavity, which results in higher mobility of oxygen anions.

Electron Paramagnetic Resonance (EPR) is known as a versatile method for characterization of active forms of oxygen present on the surface of nanocrystalline oxides. In addition to the electron-donor and electron-acceptor sites as well as O_2^- radical anions, which are observed on the surface of many finely dispersed oxide materials [40-43], unusual surface active sites with radical properties capable of generating nitroxyl radicals upon adsorption of diphenylamine have been discovered on the surface of mayenite [29, 42].

The main goal of the present study was to develop a method for producing nanocrystalline mayenite and its strontium analog after calcination at moderate temperatures for use as oxidation catalysts or catalyst supports. Several methods were studied for their synthesis and the properties of the obtained materials were characterized. The oxidative activity of the most promising samples was tested in a model reaction of diesel soot oxidation.

2. Materials and methods

The following methods were used for the synthesis of C12A7 and S12A7: calcination of a mixture of ground hydroxides (ma-method), calcination of a mixture of citrates following an adapted Pechini method (ct-method), calcination of precipitated hydroxides (sg-method) and the interaction of freshly prepared alkaline earth oxide (CaO or SrO) with an aqueous suspension of AlO(OH) (ox-method).

For the synthesis using the ma-method, stoichiometric amounts of hydroxides $M(OH)_2$ (M = Ca, Sr) and AlO(OH) (Pural SB-1, pseudo-boehmite, >99.9%, Condea, Germany) taken in the 12:14 molar ratio corresponding to the mayenite stoichiometry were ground in an agate mortar and calcined at 200 °C in the nitrogen flow. The resulting mixture was ground again and calcined at 600 or 900 °C, to obtain samples C12A7-ma and S12A7-ma.

The sol-gel synthesis method (sg-method) is based on the synthesis of mixed hydroxides by co-precipitation using ammonium hydroxide from the solutions of the corresponding nitrates. The samples prepared by this method are denoted as C12A7-sg and S12A7-sg.

In the case of the Pechini method, metal nitrates were mixed in stoichiometric quantities, and a solution of citric acid in ethylene glycol was added under stirring. The resulting mixture was evaporated at 200 °C with stirring and calcined at 600-900 °C. The obtained samples are denoted as C12A7-ct and S12A7-ct.

The ox-method was earlier developed by us for the synthesis of finely dispersed samples with mayenite as the main crystalline phase (C12A7-ox) [29, 38]. The method was shown to yield samples with the surface areas about 80 m^2/g after calcination at 500 °C. The mayenite crystalline phase content exceeded 70% according to the XRD data with the average crystallite size about 30 nm [39].

In this study the ox-method was adapted for the synthesis of S12A7 samples. They were prepared as follows. Strontium hydroxide was calcined at 900 °C for 6 h to obtain SrO. Then, SrO was quickly added under intensive mixing to AlO(OH) suspension in water to obtain a mixture of hydroxides with the stoichiometric ratio $12Sr(OH)_2$ -14AlO(OH) and stirred for 2 h. The resulting precipitate was filtered and calcined at 600 or 900 °C to obtain S12A7-ox samples.

C12A7-ox and S12A7-ox samples calcined at 600 °C characterized by relatively high surface areas and mayenite contents were used to study the activity in the oxidation of diesel soot. Before the experiment, the samples were activated for 1 h in the flow of dry oxygen at 600 °C for 1 h. Alumina sample prepared by calcination of AlO(OH) at 700 °C was used as a reference sample. It consisted of pure γ-Al_2O_3 phase with the surface area of 210 m^2/g. Also, a

C12A7-ox sample calcined in a dry argon flow denoted as C12A7-ox-Ar was prepared to study the effect of heat treatment in the inert atmosphere.

The active sites on the surface of the prepared samples were studied by EPR using an ERS-221 spectrometer (Center for Scientific Instruments Engineering, Germany). The signals of oxygen radicals were registered after additional activation of the samples in air at 500 °C for 3 h. Also diphenylamine (DPA) was used as a spin probe. Before its adsorption the samples were also activated by heating in air at 500 °C for 3 h. Then, DPA was adsorbed from $2 \cdot 10^{-2}$ M solution in toluene. The EPR spectra were registered at room temperature.

Textural characteristics of the samples were studied by low-temperature nitrogen adsorption and desorption at 77 K using a Sync 200 automatic adsorption analyzer (3P INSTRUMENTS, Germany). The samples were evacuated under dynamic vacuum (less than 1 Pa) at 300 °C for 3 h. The specific surface areas were determined by the BET method in the P/Po range from 0.1 to 0.3.

The phase composition of the samples was determined by powder X-ray diffraction (XRD) analysis using a D8 Advance diffractometer (Bruker, Germany) equipped with a CuKα radiation source and a LynxEye position sensitive detector. The data were collected in the 2θ range of 10–70 ° with a step of 0.05 ° and a collection time of 5 s.

For a model experiment on temperature-programmable oxidation, 10 mg of the catalyst was ground with 10 mg of diesel soot in an agate mortar to obtain a homogeneous gray mixture. Next, the obtained sample was placed in a quartz flow reactor (inner diameter 7 mm) and heated in the air flow (15 ml/min) in the temperature range of 100-800 °C at 10 °C/min heating rate. The catalytic activity was estimated by the peak of the CO release (Tmax) using a gas analyzer.

3. Results and Discussion

3.1. Different methods for mayenite synthesis

The classic method used for the synthesis of active mayenite structures is based on melting a mixture of precursors with the mayenite stoichiometry Ca:Al = 12:14 followed by cooling the melt to the crystallization temperature of the C12A7 phase. Other synthetic methods that potentially can be used for the mayenite synthesis are based on the preparation of a suitable precursor with the following calcination at elevated temperatures that are below the melting point to preserve the mayenite dispersity. The temperature increase generally leads to an increase in the C12A7 concentration in the sample. However, at higher temperatures the sample is subjected to sintering and a decrease in the surface area. For the strontium analog of mayenite,

very high temperatures are not suitable as the S12A7 phase is less stable at high temperatures [12].

Meanwhile, the calcination temperature required for the formation of the target phase significantly depends on the nature of the precursor. A number of synthetic techniques were tested to select the best method for synthesis of nanocrystalline C12A7 and S12A7 mayenite structures with the maximum content of the target phases while maintaining high specific surface areas. The samples obtained were studied by the XRD and low-temperature nitrogen adsorption.

Calcination of the precursors obtained by the ma-method using $M(OH)_2$-$Al(OH)_3$ mixtures made it possible to obtain C12A7 and S12A7 samples with a high yield of the mayenite phase (Table 1). It is notable that C12A7 was obtained only after calcination at 900 °C whereas the S12A7 phase was observed already after calcination at 600 °C. After calcination at 900 °C it decomposed to form S3A and SA phases in good agreement with the literature data reporting that the S12A7 phase is not stable at high temperatures [12]. However, the specific surface areas of these samples were very low (< 10 m^2/g, Table 2). Apparently the ma-method is not capable of yielding nanocrystalline samples with developed surface areas. At lower calcination temperatures the solid-phase reaction leading to the formation of the mayenite phase did not occur. Only the reflexes of the individual Ca, Sr, and Al oxides were recorded by XRD.

The Pechini method, which is widely used for the synthesis of various nanocrystalline catalysts and catalyst supports based on complex oxides, such as perovskites, appeared to be unsuitable for the mayenite synthesis. Despite all our efforts, this phase was not formed as the main crystalline phase in the samples prepared by this method until very high calcination temperatures. Easy formation of Ca or Sr carbonates after combustion of the used organic precursors might be the reason for the lack of mayenite phase after calcination at 600 or 900 °C (Table 1). Mixed calcium (or strontium) aluminate phases appeared only after calcination at 1100 °C. However, even in this case M3A ($M_3Al_2O_6$) and MA (MAl_2O_4) phases (M = Ca or Sr) were the main crystalline phases observed by XRD.

Table 1. Main crystalline phases observed by XRD in the C12A7 and S12A7 samples prepared by different methods.

Sample	Precursors		Main crystalline phases after calcination at	
	Ca/Sr	Al	600 °C	900 °C
C12A7-ma	$Ca(OH)_2$	$Al(OH)_3$	CaO	**C12A7**
C12A7-ct	$Ca(NO_3)_2$•$4H_2O$	$Al(NO_3)_3$•$9H_2O$	$CaCO_3$	CaO

C12A7-sg	$Ca(NO_3)_2•4H_2O$	$Al(NO_3)_3•9H_2O$	CaO	C3A, CA
C12A7-ox	CaO	AlOOH	**C12A7**	**C12A7**
S12A7-ma	$Sr(OH)_2$	$Al(OH)_3$	**S12A7**	S3A, SA
S12A7-ct	$Sr(NO_3)_2•4H_2O$	$Al(NO_3)_3•9H_2O$	$SrCO_3$	$SrCO_3$
S12A7-sg	$Sr(NO_3)_2•4H_2O$	$Al(NO_3)_3•9H_2O$	S3A	S3A
S12A7-ox	SrO	AlOOH	**S12A7**	S3A, SA

C12A7-ox and S12A7-ox samples calcined in air at 600 °C had C12A7 and S12A7 as predominant crystalline phases. The XRD patterns of these samples are shown in Fig. 1. CaO is the main impurity observed in a small amount in the XRD pattern of C12A7-ox. Weak signals of S3A and $SrCO_3$ are observed in the XRD pattern of S12A7-ox in addition to the S12A7 phase. The lines in the S12A7-ox diffraction pattern are narrower than those of C12A7-ox suggesting that the average size of its crystallites is larger. The average crystallite sizes determined by the Scherrer equation are 14 and 25 nm for C12A7-ox and S12A7-ox samples, respectively.

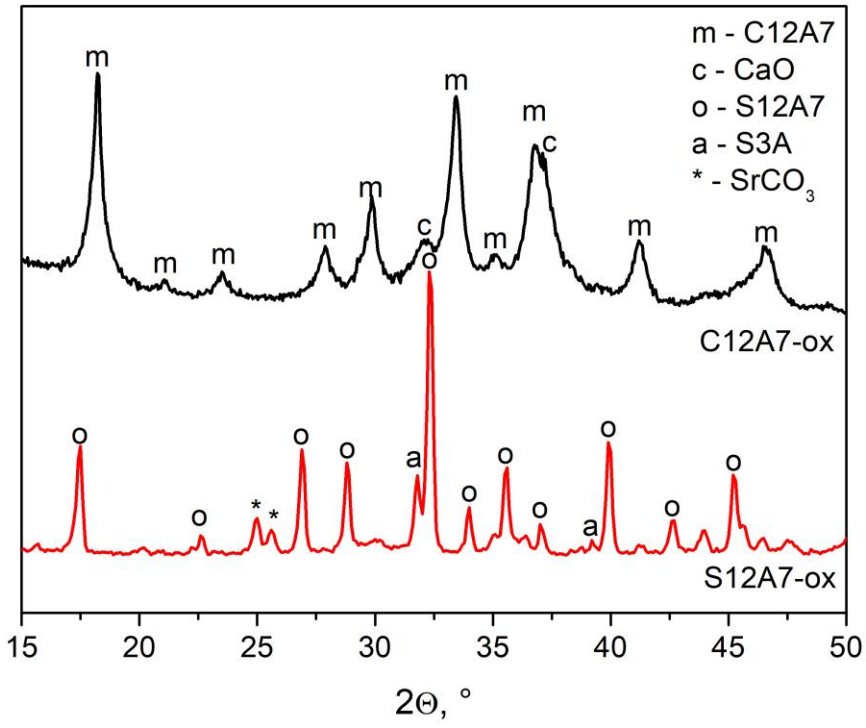


Fig. 1 XRD patterns of C12A7-ox and S12A7-ox samples calcined at 600 °C

Both samples calcined at 600 °C had relatively high specific surface areas: 80 and 68 m^2/g for C12A7-ox and S12A7-ox, respectively (Table 2). So, these samples seem to be suitable for application as catalysts or catalyst supports. After calcination at 900 °C the surface area of

C12A7-ox sample decreased to 25 m^2/g, mayenite remaining its main crystalline phase. Meanwhile, calcination of S12A7-ox at 900 °C resulted in complete decomposition of the S12A7 phase with the formation of S3A ($Sr_3Al_2O_6$) and SA ($SrAl_2O_4$ phases (Table 1).

Table 2. Specific surface areas of selected samples.

Sample	Calcination temperature, °C	Main crystalline phase	S_{BET}, m^2/g
C12A7-ma	900	C12A7	8
C12A7-ox	600	C12A7	80
C12A7-ox	900	C12A7	25
S12A7-ma	600	S12A7	5
S12A7-ox	600	S12A7	68

3.2. EPR study of C12A7-ox and S12A7-ox

The most interesting samples C12A7-ox and S12A7-ox calcined at 600 °C were characterized by EPR. The positive charge of the mayenite frameworks synthesized at low temperatures is compensated by hydroxyl anions. The oxidizing properties of such materials are quite weak. Calcination of such samples at higher temperatures under inert atmosphere results in gradual decomposition of the hydroxyl form leading to the formation of mayenite where O^{2-} anions compensate the positive charge of the framework. In the presence of oxygen, O_2 molecules can penetrate into the framework starting from 600 °C resulting in the appearance the EPR signal attributed to the simultaneous presence of O_2^- and O^- radicals [17, 18]. These active radical species can be detected by EPR spectroscopy, which makes this method convenient for characterizing the oxidative properties of a material.

Figure 2 shows the EPR spectra of C12A7-ox and S12A7-ox calcined in air at 600 °C. The signal attributed to the simultaneous presence of O_2^- and O^- radicals was observed on both samples. The appearance and parameters of this signal are consistent with the earlier reported data where it was concluded that is could be explained by a superposition of the spectra of O_2^- radicals (g_{xx} = 2.002, g_{yy} = 2.008, g_{zz} = 2.074) and O^- radicals ($g_{xx} = g_{yy}$ = 2.036, g_{zz} = 1.994) [12, 18, 27, 44]. Such signal was not observed if the samples were calcined in the argon flow.

The peak-to-peak intensity of this signal in the spectrum of S12A7-ox is approximately 3 times higher than in the case of C12A7-ox whereas the shapes and widths of the signals are quite similar (Fig. 2). This result implies that the concentration of radical species in the Sr-containing sample is higher despite its lower surface area. This result can be due to easier penetration of oxygen molecules into the S12A7 framework. Both signals are relatively weak compared to the signals earlier reported for samples calcined at very high temperatures where

significant O_2 penetration into the framework takes place [18]. Most likely, in the case of samples calcined at 600 °C their penetration is hampered by the predominant presence of OH^- ions as the charge compensating anions. Still, one can expect that the oxygen radicals are mostly located close to the surface of the nanocrystals making it easier for them to take part in various reactions.

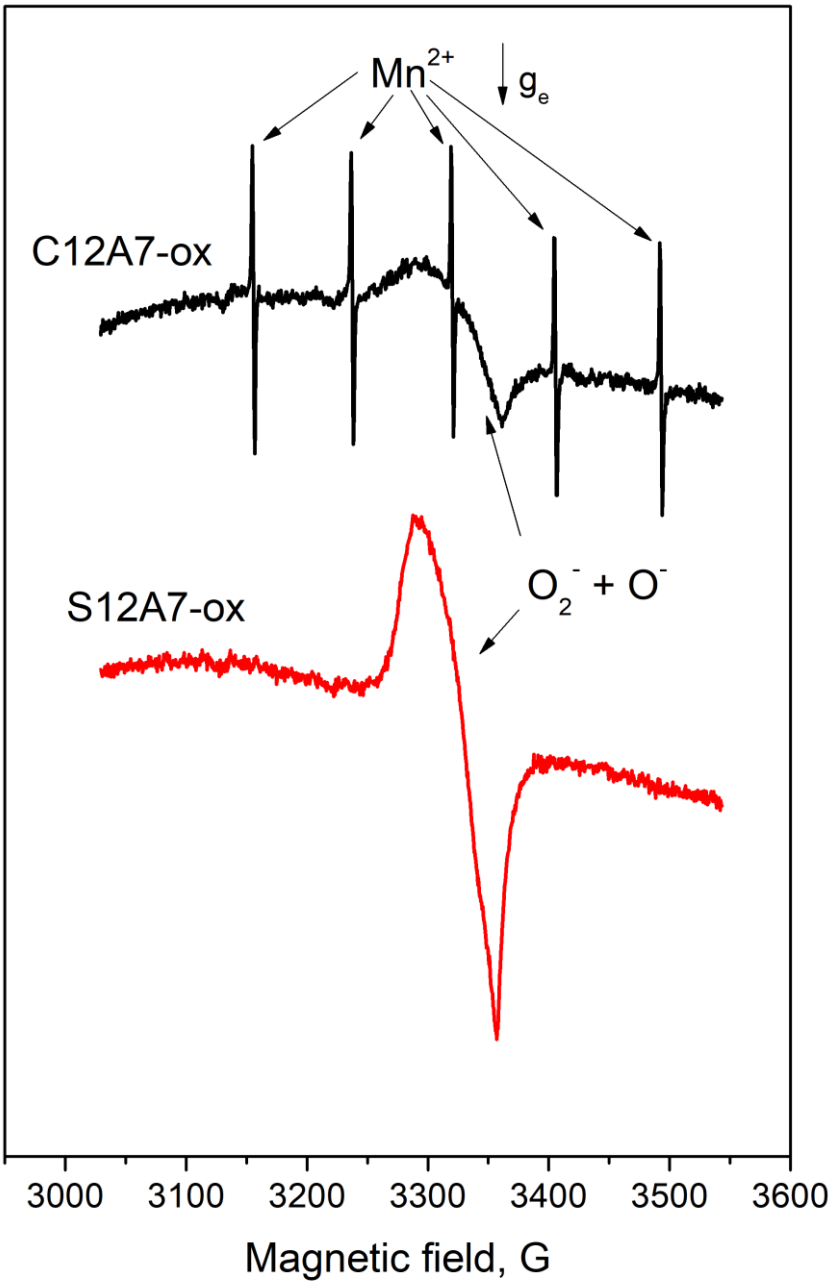


Fig. 2 EPR spectra of C12A7-ox and S12A7-ox calcined in air at 600 °C

A well-known 6-line signal attributed to Mn^{2+} impurity ions present in the cubic coordination in the CaO phase [45,46] was also observed in the EPR spectrum of C12A7-ox. Only 5 lines of this spectrum can be seen in Fig. 2 because the sixth line falls out of the field range where the spectra were registered. CaO was detected by XRD as an impurity phase present in this sample (Fig. 1). This signal was not observed for S12A7-ox where the SrO phase was not registered by XRD.

The EPR spectra observed after the DPA adsorption on C12A7-ox and S12A7-ox feature a frozen triplet with hyperfine splitting on a single nitrogen atom with the splitting constant A_{zz}=16 G (Fig. 3). This triplet can be attributed to the diphenyloxyl nitroxyl radicals adsorbed on the surface of the samples. Similar signals were earlier reported for different dispersed samples containing the mayenite phase [29, 42]. Meanwhile, it is not typical for other oxide catalysts and supports. This is the first time such a signal is reported for S12A7. The signal intensities on these samples are very similar with radical concentrations determined by double integration of the spectra close to 1.0 μmol/g. The formation of these radicals indicates that a noticeable concentration of radicals, which are capable to detach the hydrogen atom from the nitrogen atom of the spin probe molecule, exist on the surface of nanocrystalline C12A7-ox and S12A7-ox samples.

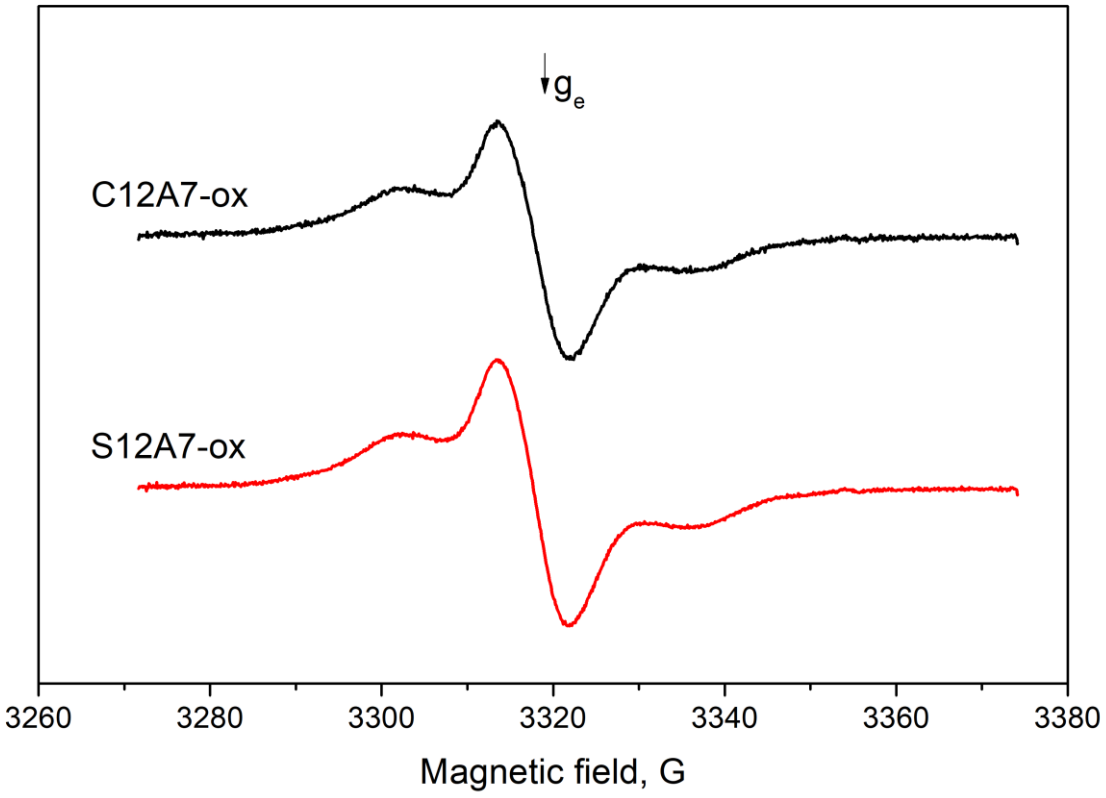


Fig. 3 EPR spectra observed on the surface of C12A7-ox and S12A7-ox calcined in air at 600 °C after adsorption of diphenylamine

3.3. Investigation of the catalytic activity in diesel soot oxidation

The data reported above suggest that C12A7-ox and S12A7-ox are the most promising samples for application as oxidation catalysts. They have reasonably high surface areas and considerable concentrations of oxygen radicals on their surface. Their oxidative activity was evaluated in temperature-programmed oxidation of diesel soot performed in the temperature range of 200-800 °C. The temperature maximum of the carbon monoxide release was used as the main parameter of catalytic activity. CO is usually formed as a by-product during the soot oxidation in addition to CO_2, which is the main product [4, 47]. The volume of CO released at different temperatures during the temperature-programmed oxidation was reported to correlate with the volume of CO_2 [7, 8]. The obtained results are shown in Fig. 4. The shift of the CO emission peak to lower temperatures corresponds to samples more active in the soot oxidation. Complete discoloration of the samples was observed at the end of the process indicating quantitative oxidation of the soot sample.

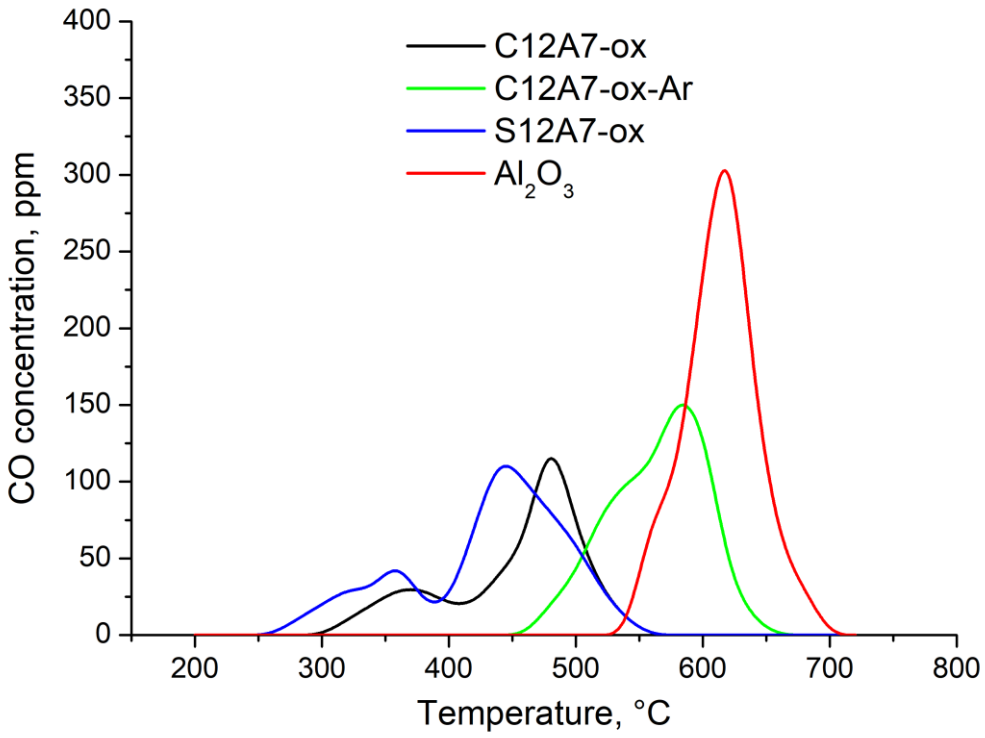


Fig. 4 Investigation of the catalytic activity in temperature-programmed oxidation of diesel soot

Both C12A7-ox and S12A7-ox were characterized by higher activity than Al_2O_3. For Al_2O_3 the CO release peak was observed at 620 °C (Fig. 4). This is the typical temperature range where non-catalytic soot combustion takes place [1]. Meanwhile, C12A7-ox and S12A7-ox activated in air at 600 °C showed much higher catalytic activity with Tmax equal to 480 and 440 °C, respectively. The ignition temperatures where the first CO release was observed were 320 °C and 280 °C, respectively.

Overall, soot oxidation takes place on the catalysts explored in this study approximately in the same temperature range as on such popular catalysts actively studied for soot oxidation as CeZrOx and perovskites [1, 2, 4, 6]. Although Tmax values obtained in this study for C12A7-ox and S12A7-ox are somewhat higher than those reported for the most efficient modified catalysts based on CeO_2 or perovskites [1, 48-50], nanocrystalline C12A7 and S12A7 achieve the temperature range of practical interest for soot oxidation without any modification with noble or transition metals. It leaves room for further improvement using modification with transition metals similar to that reported for C12A7 doped with Cu, which was shown to improve significantly the catalytic activity of mayenite in soot oxidation [8].

The higher oxidation activity of mayenite samples is consistent with the presence of oxygen radical anions observed by EPR. It should be noted that an increase in the concentration of oxygen radical anions leads to easier oxidation of soot deposited on the surface. S12A7-ox proved to be more effective in this process. Presumably, the wider unit cell of the S12A7 framework compared with C12A7 leads to greater mobility of O_2^- radical anions and, consequently, higher catalytic activity. This makes S12A7 a promising material for use as a catalyst or catalyst support that has been barely explored so far [51].

Note that C12A7-ox treated in Ar had substantially higher Tmax = 580 °C (Fig. 4). The lower activity of this sample can be explained by the lack of oxygen radicals on its surface. Apparently, this sample gradually becomes catalytically active as such radicals start forming already during the catalytic reaction at temperatures above 500 °C.

Overall, nanocrystalline C12A7 and S12A7 prepared by reaction of alkaline earth oxides (CaO or SrO) with an aqueous suspension of AlO(OH) are interesting materials deserving further investigation in various catalytic oxidation processes. They do not require deposition of noble metals and can be used either in the pristine form or as supports for transition metals.

4. Conclusions

The synthesis of nanocrystalline mayenite ($Ca_{12}Al_{14}O_{33}$) and its Sr analog ($Sr_{12}Al_{14}O_{33}$) at moderate temperatures was attempted by several methods. The most promising results were obtained using the reactions of CaO or SrO with water in the presence of AlOOH. After calcination at 600 °C, mayenite and its Sr analog were the predominating crystalline phases in the C12A7 and S12A7 samples prepared by this method. Nanocrystalline S12A7 sample with the surface area of 68 m^2/g was prepared for the first time using this method. According to the EPR data, these samples had active oxygen radical species on the surface after activation in air. They proved to be active in the temperature-programmed soot oxidation showing substantially higher activity than the Al_2O_3 sample used as a reference material. The Sr-containing sample demonstrated higher activity than C12A7-ox with the CO release peak at 440 °C, most likely, due to wider crystalline cell and enhanced mobility of extra-framework oxygen anions. Thus, nanocrystalline mayenite C12A7 and its Sr analog S12A7 are promising materials for soot oxidation without the presence of noble metals.

Author contributions

Anton P. Koskin: Conceptualization, Methodology, Investigation, Formal analysis, Writing – original draft. Ekaterina I. Shuvarakova: Investigation, Visualization. Alexander F. Bedilo: Methodology, Investigation, Formal analysis, Writing – original draft.

Acknowledgment

This study was supported by the Russian Science Foundation (Project 25-23-00455).

Competing Interests

The authors have no competing interests to declare that are relevant to the content of this article

Data availability statement

The data that support the findings of this study are available from the corresponding author upon reasonable request

References

1. Legutko P, Stelmachowski P, Yu X, Zhao Z, Sojka Z, Kotarba A (2023) Catalytic soot combustion - general concepts and alkali promotion. ACS Catal 13:3395-3418. https://doi.org/10.1021/acscatal.2c05994
2. Zhang X, Chen X, Chen S, Zhou S, Wang L, Zhang C, Gao S, Yu D, Fan X, Cheng Y, Yu X, Zhao Z (2024) Research progress on the preparation of alkali/alkaline earth metal-modified metal oxide catalysts and their application to diesel engine exhaust soot particle catalytic purification. Surf Interfaces 49:104410. https://doi.org/10.1016/j.surfin.2024.104410
3. Tu Z, Wu G, Zheng C, Wu X, Wan J, Liu S (2025) Perspective about gasoline soot combustion over ceria catalysts: A close look into the “active oxygen” enigma. J Rare Earths 43:641-659. https://doi.org/10.1016/j.jre.2024.08.017
4. Yang Z, Chen Z, Zhang N, Zhou Y, Luo D, Jin T, Zhang H (2025) Time-dependent evolution of morphologies and lattice defects in hydrothermal synthesized ceria-zirconia solid solutions for catalytic combustion of diesel soot. Fuel Process Technol 276:108294 . https://doi.org/10.1016/j.fuproc.2025.108294
5. Ma Y, Guo H, Xiong J, Xu L, Wei Y (2024) Research Advances in Rare Earth Oxide-Based Catalysts for Soot Combustion. ChemCatChem 16:e202301317. https://doi.org/10.1002/cctc.202301317
6. Guan B, Chen J, Zhuang Z, Zhu L, Ma Z, Hu X, Zhu C, Zhao S, Shu K, Dang H, Gao J, Zhang L, Zhu T, Huang Z (2025) Experimental study on the soot oxidation activity and sulfur poisoning resistance of $CuCeZrO_{2-\delta}$ catalyst. Mater Chem Phys 345:131244. https://doi.org/10.1016/j.matchemphys.2025.131244
7. Meza-Trujillo I, Devred F, Gaigneaux EM (2019) Production of high surface area mayenite (C12A7) via an assisted solution combustion synthesis (SCS) toward catalytic soot oxidation. Mater Res Bull 119:110542. https://doi.org/10.1016/j.materresbull.2019.110542
8. Meza-Trujillo I, Mary A, Pietrzyk P, Sojka Z, Gaigneaux EM (2022) Nature and role of Cu(II) species in doped C12A7 catalysts for soot oxidation. Appl Catal B: Environ 316:121604. https://doi.org/10.1016/j.apcatb.2022.121604
9. Shkerin SN, Tolkacheva AS (2022) Mayenite (A Review). Rus J Gen Chem 92:2312-2333. https://doi.org/10.1134/S1070363222110160

10. Zhang X, Li Z, Xu M, Hosono H, Ye TN (2023) Recent progress and prospects in active anion-bearing C12A7-mediated chemical reactions. J Mater Chem A 11:15074-15099. https://doi.org/10.1039/d3ta02422a
11. Yamaguchi O, Narai A, Shimizu K (1986) New compound in the system SrO-Al_2O_3. J Am Ceram Soc 69:C-36-C-37. https://doi.org/https://doi.org/10.1111/j.1151-2916.1986.tb04732.x
12. Hayashi K, Ueda N, Matsuishi S, Hirano M, Kamiya T, Hosono H (2008) Solid state syntheses of $12SrO{\cdot}7Al_2O_3$ and formation of high density oxygen radical anions, O^- and O_2^-. Chem Mater 20:5987-5996. https://doi.org/10.1021/cm800666p
13. Salasin JR, Rawn C (2017) Structure property relationships and cationic doping in $[Ca_{24}Al_{28}O_{64}]^{4+}$ framework: A review. Crystals 7:143. https://doi.org/10.3390/cryst7050143
14. Yang S, Kondo JN, Hayashi K, Hirano M, Domen K, Hosono H (2004) Formation and desorption of oxygen species in nanoporous crystal $12CaO{\cdot}7Al_2O_3$. Chem Mater 16:104-110. https://doi.org/10.1021/cm034755r
15. Hosono H, Abe Y (1987) Occurrence of superoxide radical ion in crystalline $12CaO{\cdot}7Al_2O_3$ prepared via solid-state reactions. Inorg Chem 26:1192-1195. https://doi.org/10.1021/ic00255a003
16. Hosono H, Hayashi K, Kajihara K, Sushko PV, Shluger AL (2009) Oxygen ion conduction in $12CaO{\cdot}7Al_2O_3$: O_2^- conduction mechanism and possibility of O^- fast conduction. Solid State Ion 180:550-555. https://doi.org/10.1016/j.ssi.2008.10.015;Article
17. Hayashi K, Ueda N, Hirano M, Hosono H (2004) Effect of stability and diffusivity of extra-framework oxygen species on the formation of oxygen radicals in $12CaO{-}7Al_2O_3$. Solid State Ion 173:89-94. https://doi.org/10.1016/j.ssi.2004.07.057
18. Hayashi K, Matsuishi S, Ueda N, Hirano M, Hosono H (2003) Maximum incorporation of oxygen radicals, O^- and O_2^-, into $12CaO{\cdot}7Al_2O_3$ with a nanoporous structure. Chem Mater 15:1851-1854. https://doi.org/10.1021/cm020959g
19. Hayashi F, Toda Y, Kanie Y, Kitano M, Inoue Y, Yokoyama T, Hara M, Hosono H (2013) Ammonia decomposition by ruthenium nanoparticles loaded on inorganic electride C12A7:e^-. Chem Sci 4:3124-3130. https://doi.org/10.1039/c3sc50794g
20. Kammert J, Moon J, Cheng Y, Daemen L, Irle S, Fung V, Liu J, Page K, Ma X, Phaneuf V, Tong J, Ramirez-Cuesta AJ, Wu Z (2020) Nature of reactive hydrogen for ammonia

synthesis over a Ru/C12A7 electride catalyst. J Am Chem Soc 142:7655-7667. https://doi.org/10.1021/jacs.0c02345

21. Li J, Kitano M, Ye TN, Sasase M, Yokoyama T, Hosono H (2017) Chlorine-tolerant ruthenium catalyst derived using the unique anion-exchange properties of 12 CaO- 7 Al_2O_3 for ammonia synthesis. ChemCatChem 9:3078-3083. https://doi.org/10.1002/cctc.201700353
22. Peng R, Chen Y, Zhang B, Li Z, Cui X, Guo C, Zhao Y, Zhang J (2021) Tailoring the stability of Ni-Fe/mayenite in methane - carbon dioxide reforming. Fuel 284:118909. https://doi.org/10.1016/j.fuel.2020.118909
23. Yang S, Kondo JN, Hayashi K, Hirano M, Domen K, Hosono H (2004) Partial oxidation of methane to syngas over promoted C12A7. Appl Catal A: Gen 277:239-246. https://doi.org/10.1016/j.apcata.2004.09.030
24. Dang C, Yu H, Wang H, Peng F, Yang Y (2016) A bi-functional Co-CaO-$Ca_{12}Al_{14}O_{33}$ catalyst for sorption-enhanced steam reforming of glycerol to high-purity hydrogen. Chem Eng J 286:329-338. https://doi.org/10.1016/j.cej.2015.10.073
25. Dang C, Xia H, Yuan S, Wei X, Cai W (2022) Green hydrogen production from sorption-enhanced steam reforming of biogas over a Pd/Ni-CaO-mayenite multifunctional catalyst. Renew Energy 201:314-322. https://doi.org/10.1016/j.renene.2022.10.106
26. Li C, Hirabayashi D, Suzuki K (2009) A crucial role of O_2^- and O_2^{2-} on mayenite structure for biomass tar steam reforming over Ni/$Ca_{12}Al_{14}O_{33}$. Appl Catal B: Environ 88:351-360. https://doi.org/10.1016/j.apcatb.2008.11.004
27. Matsuishi S, Toda Y, Miyakawa M, Hayashi K, Kamiya T, Hirano M, Tanaka I, Hosono H (2003) High-density electron anions in a nanoporous single crystal: $[Ca_{24}Al_{28}O_{64}]^{4+}$ ($4e^-$). Science 301:626-629. https://doi.org/10.1126/science.1083842
28. Ilyina EV, Gerus YY, Cherepanova SV, Bedilo AF (2021) Synthesis of C12A7 calcium aluminate aerogels. Mater Lett 293:129699. https://doi.org/10.1016/j.matlet.2021.129699
29. Shuvarakova EI, Bedilo AF, Kenzhin RM, Ilyina EV, Gerus YY (2022) Synthesis and investigation of finely dispersed calcium aluminates and catalysts based on them. Rus J Phys Chem B 16:411-420. https://doi.org/10.1134/S199079312203023X
30. Ilyina EV, Kapishnikov AV, Serkova AN, Shuvarakova EI, Bedilo AF (2026) Effect of toluene on the formation of nanocrystalline mayenite phase by the sol-gel method. J Sol-Gel Sci Technol 117:6. https://doi.org/10.1007/s10971-025-07080-1

31. Gong L, Lin Z, Ning S, Sun J, Shen J, Torimoto Y, Li Q (2010) Synthesis and characteristics of the C12A7-O^- nanoparticles by citric acid sol-gel combustion method. Mater Lett 64:1322-1324. https://doi.org/10.1016/j.matlet.2010.03.023
32. Matovic B, Prekajski M, Pantic J, Brauniger T, Rosic M, Zagorac D, Milivojevic D (2016) Synthesis and densification of single-phase mayenite (C12A7). J Eur Ceram Soc 36:4237-4241. https://doi.org/10.1016/j.jeurceramsoc.2016.06.014
33. Salasin JR, Schwerzler SEA, Koehler MR, Keffer DJ, Rawn CJ (2018) The effect of process parameters on the amorphous citrate sol-gel synthesis of Cu-doped $Ca_{12}Al_{14}O_{33}$. Materialia 4:466-477. https://doi.org/10.1016/j.mtla.2018.11.003
34. Berent K, Komarek S, Lach R, Pyda W (2019) The effect of calcination temperature on the structure and performance of nanocrystalline mayenite powders. Materials 12:3476. https://doi.org/10.3390/ma12213476
35. Hasegawa G, Moriya S, Inada M, Kitano M, Okunaka M, Yamamoto T, Matsukawa Y, Nishimi K, Shima K, Enomoto N, Matsuishi S, Hosono H, Hayashi K (2018) Topotactic synthesis of mesoporous $12CaO{\cdot}7Al_2O_3$ mesocrystalline microcubes toward catalytic ammonia synthesis. Chem Mater 30:4498-4502. https://doi.org/10.1021/acs.chemmater.8b01819
36. Jimenez A, Rives V, Vicente MA (2022) Thermal study of the hydrocalumite - katoite - calcite system. Thermochim Acta 713:179242. https://doi.org/10.1016/j.tca.2022.179242
37. Li C, Hirabayashi D, Suzuki K (2011) Synthesis of higher surface area mayenite by hydrothermal method. Mater Res Bull 46:1307-1310. https://doi.org/10.1016/j.materresbull.2011.03.023
38. Kapishnikov AV, Kenzhin RM, Koskin AP, Volodin AM, Geydt PV (2022) Mayenite synthesis from hydroxide precursors: structure formation and active sites on its surface. Materials 15:778. https://doi.org/10.3390/ma15030778
39. Kapishnikov AV, Shuvarakova EI, Cherepanova SV, Gerasimov EY, Bespalko YN, Maksimovskiy EA, Volodin AM, Bedilo AF (2025) Effect of the phase composition of Ca-Al hydroxide precursors on the mayenite formation. Ceram Int 51:35496-35505. https://doi.org/10.1016/j.ceramint.2025.05.272
40. Bedilo AF, Shuvarakova EI, Rybinskaya AA, Medvedev DA (2014) Characterization of electron-donor and electron-acceptor sites on the surface of sulfated alumina using spin probes. J Phys Chem C 118:15779-15794. https://doi.org/10.1021/jp503523k

41. Bedilo AF, Shuvarakova EI, Volodin AM, Ilyina EV, Mishakov IV, Vedyagin AA, Chesnokov VV, Heroux DS, Klabunde KJ (2014) Effect of modification with vanadium or carbon on destructive sorption of halocarbons over nanocrystalline MgO: The role of active sites in initiation of the solid-state reaction. J Phys Chem C 118:13715-13725. https://doi.org/10.1021/jp503916e
42. Volodin AM, Bedilo AF, Stoyanovskii VO, Zaikovskii VI (2018) High-temperature synthesis of finely dispersed oxide materials and C12A7:e electrides in carbon nanoreactor conditions. Nanosystems: Phys Chem Math 9:558-567. https://doi.org/10.17586/2220-8054-2018-9-4-558-567
43. Koskin AP, Andreev RV, Primachenko ON, Shuvarakova EI, Bedilo AF (2020) Perfluorosulfonic Acid Polymer Composites: Effect of the Support and Synthesis Method on the Acid and Catalytic Properties. Mol Catal 492 111006:1-9. https://doi.org/10.1016/j.mcat.2020.111006
44. Hayashi K, Hirano M, Matsuishi S, Hosono H (2002) Microporous crystal $12CaO{\cdot}7Al_2O_3$ encaging abundant O^- radicals. J Am Chem Soc 124:738-739. https://doi.org/10.1021/ja016112n
45. Rubio OJ, Munoz PE, Boldu OJ, Chen Y, Abraham MM (1979) EPR powder pattern analysis for Mn^{2+} in cubic crystalline fields. J Chem Phys 70:633-638. https://doi.org/10.1063/1.437542
46. Livraghi S, Paganini MC, Giamello E (2011) EPR study of electron trapping on partially hydroxylated alkali-earth oxides occurring during SO_2 disproportionation. J Mol Catal A: Chem 349:100-104. https://doi.org/10.1016/j.molcata.2011.08.004
47. Zhang Z, Chen J, Zhang C, Yu W (2026) Soot reactivity and regeneration mechanism of modern automobile engines and methods of reducing soot emission for diesel particulate filter: A review. Fuel Process Technol 287:108458. https://doi.org/10.1016/j.fuproc.2026.108458
48. Zhang W, Niu X, Chen L, Yuan F, Zhu Y (2016) Soot combustion over nanostructured ceria with different morphologies. Sci Rep 6:29062. https://doi.org/10.1038/srep29062
49. Neha, Singh SV (2022) Facile and template-free synthesis of nano-macroporous $LaCoO_3$ perovskite oxide for efficient diesel soot oxidation. React Kinet Mech Catal 135:1607-1620. https://doi.org/10.1007/s11144-022-02219-5
50. Ivanova TV, Homola T, Bryukvin A, Cameron DC (2018) Catalytic performance of Ag_2O and Ag doped CeO_2 prepared by atomic layer deposition for diesel soot oxidation. Coatings 8:237. https://doi.org/10.3390/coatings8070237

51. Iida H, Onuki N, Numa T, Igarashi A (2016) Steam reforming of dodecane and toluene over Ru/12SrO-7Al_2O_3 (S12A7) catalysts. Fuel Process Technol 142:397-402. http://doi.org/10.1016/j.fuproc.2015.09.026